Nucleic Acids Research, 2001, Vol. 29, No. 15 **3219–3230**

Re-examination of the intrinsic, dynamic and hydration properties of phosphoramidate DNA

Nilesh K. Banavali and Alexander D. MacKerell Jr*

Department of Pharmaceutical Sciences, School of Pharmacy, University of Maryland, 20 North Pine Street, Baltimore, MD 21201, USA

Received April 11, 2001; Revised and Accepted June 12, 2001

ABSTRACT

Intrinsic energetic and solvation factors contributing to the unusual structural and biochemical properties of N3′-phosphoramidate DNA analogs have been re-examined using a combination of quantum mechanical and molecular dynamics methods. Evaluation of the impact of the N3′-H substitution was performed via comparison of N3′-phosphoramidate DNA starting from both A- and B-form structures, B-form DNA and A-form RNA. The N3′-H group is shown to be flexible, undergoing reversible inversion transitions associated with motion of the hydrogen atom attached to the N3′ atom. The inversion process is correlated with both sugar pucker characteristics as well as other local backbone torsional dynamics, yielding increased dihedral flexibility over DNA. Solvation of N3′-phosphoramidate DNA is shown to be similar to RNA, consistent with thermodynamic data on the two species. A previously unobserved intrinsic conformational perturbation caused by the N5′-phosphoramidate substitution is identified and suggested to be linked to the differences in the properties of N3′- and N5′-phosphoramidate oligonucleotide analogs.

INTRODUCTION

Oligonucleotide analogs can be used as antisense therapeutic agents that block disease gene expression by binding complementary mRNA single strands (1,2). N3′-DNA analogs are oligonucleotide analogs which show most of the desirable properties of antisense agents, including high complementary strand binding affinity for DNA/RNA, nuclease resistance and good solubility (3). A good example of their antisense ability is seen in their strong and specific *in vitro* inhibition of HIV-1 reverse transcription by hybridization to HIV-1 TAR RNA (4). In addition to forming duplexes with complementary single-stranded DNA or RNA, they have the ability to inhibit transcription by forming stable triple helices with duplex DNA (2). These DNA analogs can even mimic RNA in their binding to RNA-binding proteins, thereby inhibiting the activity of these proteins (5). An interesting example of their adaptability is the ability to utilize tertiary interactions, distinct from base pairing interactions, for *in vitro* suicide inhibition of self-splicing of an intron (6,7). The use of N3′-DNA antisense oligonucleotides in c-*myc* gene inhibition has even been shown to have an anti-leukemia effect *in vivo* (8). Such widely demonstrated *in vitro* and *in vivo* efficacy of N3′-DNA analogs makes them very promising antisense agents. For future rational design of better antisense agents, however, it is first essential to understand the factors that contribute to these favorable biochemical properties at an atomic level.

An important difference between regular DNA and N3′-DNA that may be related to the observed biochemical changes is the A-form preference of N3′-DNA in aqueous solution (9). This unusual structural property of N3′-DNA analogs has been addressed in previous theoretical studies (10–12). In addition, both the crystallographic and NMR structures of an N3′-DNA dodecamer have been solved (13,14). Various suggestions put forth to explain this phenomenon include specific anomeric effects (13), a C3′-*endo* (or north) sugar pucker preference due to reduced electronegativity of the 3′-substituent (11) and differential hydration effects (10). In a recent study using quantum mechanical methods (15), we demonstrated that the anomeric effect in the N3′-phosphoramidate backbone was more complex than previously stated (13). Additionally, as shown by results in the present study, whether the C3′-*endo* conformation of the N3′-substituted sugars is a result of intrinsic changes or solvent-induced changes in energetics is also not a trivial consideration. Solvation is also known to influence the anomeric effect (15,16) as well as the conformational properties of sugars (17). It is clear that a complex interrelationship exists between these factors which needs to be explored further to understand the reasons behind the unusual properties of N3′-phosphoramidate analogs.

One aspect of N3′-phosphoramidate structure that is intricately linked to the factors discussed above and has not been emphasized in previous studies is the flexibility of the N3′-H moiety in N3′-phosphoramidates. The flexibility and the exchangeability of the N3′ hydrogen with solvent has only been mentioned briefly in the NMR structure determination study (14). In a previous molecular dynamics investigation, the dynamics of the N3′-phosphoramidate was seen to be dependent on the initial conformation assigned to the N3′-H moiety, however, this was suggested to be an anomaly (11). To understand this issue, it is essential to note that the N3′-H

*To whom correspondence should be addressed. Tel: +1 410 706 7442; Fax: +1 410 706 0346; Email: alex@outerbanks.umaryland.edu
Present address:
Nilesh K. Banavali, W-205, Department of Biochemistry, Weill Medical College of Cornell University, 1300 York Avenue, New York, NY 10021, USA

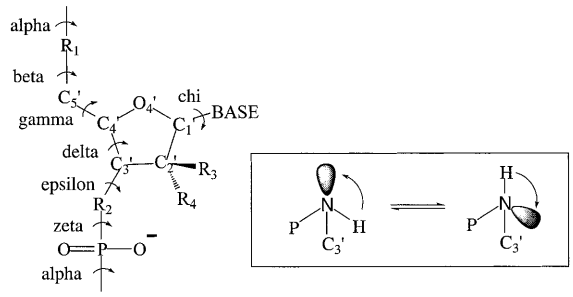

	R_1	R_2	R_3	R_4	Initial Sugar pucker
A. ARNA	O	O	H	OH	C3'-endo/north
B. BDNA	O	O	H	H	C2'-endo/south
C. N3'ADNA	O	NH	H	H	C3'-endo/north
D. N3'BDNA	O	NH	H	H	C2'-endo/south
E. N5'-DNA	NH	O	H	H	Not applicable

Figure 1. Structural and chemical differences between the sugar moiety in ARNA, BDNA, N3′-DNA and N5′-DNA and the associated nomenclature of backbone dihedral degrees of freedom. (Inset) Amino inversion and the C-P-N-H improper dihedral angle

moiety mostly assumes a tetrahedral conformation in N3′-phosphoramidates (Fig. 1, inset). The tetrahedral conformation leads to chirality about the N3′ atom since it is connected to four different functional groups (the lone pair of electrons being one of them). Rehybridization (or inversion) around the N atom can occur such that the hydrogen and the lone pair positions are exchanged. This phenomenon and its effects on the conformational properties of the N3′-H moiety have been studied using quantum mechanical (QM) calculations on small model compounds (15), however, the effects on macromolecular structure and properties are practically impossible to study using QM methods due to the enormous computational cost involved. Molecular dynamics (MD) simulations provide an attractive alternative to study the atomic level intrinsic and solvation properties of macromolecules. However, the inability to represent electronic degrees of freedom in the atomic model used in MD prevents explicit treatment of such rehybridization or inversion phenomena. For practical purposes, however, it may not be necessary to model the motion of the lone pair of electrons to treat the flexibility of the N3′-H moiety. An approximation used in the present study is to reduce the problem to treatment of the motion of the hydrogen on the N3′ atom alone. The idea motivating this approximation is that the dynamics of the lone pair and its effects on solute and solvent dynamics can be represented implicitly while the motion of the hydrogen is represented explicitly. It is possible to generate a combination of dihedral and improper dihedral parameters that can reproduce the energetic changes associated with the motion of the hydrogen, as determined from *ab initio* calculations on small model compounds, as accurately as possible in an atomic model. The consequences of this microscopic motion on the global solvation and dynamic properties of the N3′-phosphoramidate oligonucleotide analogs can then be judged using MD investigations.

The fact that inversion of the N3′-H moiety is a significant structural change at the microscopic level suggests that ignoring the flexibility of the N3′-H moiety may seriously affect determination of the underlying thermodynamic and biochemical properties. Therefore, the approach used in this study is to parameterize the CHARMM molecular mechanics force field to correctly reproduce the local flexibility changes involved in the N3′-H substitution using both *ab initio* and experimental results as target data. Particular attention is given to reproduction of the intrinsic sugar conformational energetics of the N3′-phosphoramidate substituted DNA backbone, such that only a small stabilization of the sugar conformation is introduced to reproduce the A-form conformational preference. The newly developed parameters are then utilized in MD studies to understand the impact of these local perturbations on the structural, dynamic and hydration characteristics of N3′-DNA. These properties are compared between A-form N3′-DNA, B-form N3′-DNA, A-form RNA and B-form DNA in the same environment to gain a better understanding of the A-form preference of N3′-DNA.

A related and pertinent fact is that a change in the location of the N-H substitution in the oligonucleotide backbone leads to a drastic change in the properties of the phosphoramidate oligonucleotides. Specifically, the N5′-H substitution (substitution of the O5′ atom with N5′-H) yields N5′-phosphoramidate DNA analogs which do not hybridize to form duplexes with the complementary DNA/RNA (3), making them useless as antisense agents. A possible relationship between this local change and observed properties is suggested by demonstrating a previously unidentified perturbation in the local conformational properties of the γ dihedral of the N5′-phosphoramidate backbone.

MATERIALS AND METHODS

Molecular mechanics force field calculations were carried out using the CHARMM program (18,19). The CHARMM27 parameters for DNA and RNA (20,21) were used for all calculations along with the CHARMM-modified TIP3P water model (22,23) and the sodium parameters from Beglov and Roux (24). The new parameters for N3′-DNA were developed based on *ab initio* data on various model compounds representative of N3′-phosphoramidate substituted DNA. *Ab initio* calculations were performed on the model compounds (Fig. 1) using GAUSSIAN94 (25) and GAUSSIAN98 (26) at the Hartree–Fock (HF) or second order Møller–Plesset (MP2) levels of theory with the 6-31G* basis set for neutral compounds and the 6-31+G* basis set for anionic compounds. The dihedral energy surfaces were obtained by individually constraining the specific dihedral to multiples of 30° from 0° to 360° and allowing the rest of the molecule to relax to the optimum geometry. For compounds containing a furanose sugar moiety, the C2′-*endo*, C3′-*endo* and O4′-*endo* conformations were obtained by constraining the endocyclic dihedrals C3′-C4′-O4′-C1′, C4′-O4′-C1′-C2′ and C1′-C2′-C3′-C4′, respectively, to 0.0°, as previously described (27). The chirality introduced by the tetrahedral nature of the nitrogen atom in the phosphoramidate backbone allowed for two possible orientations of the hydrogen on the nitrogen. The transformation of one orientation to another through amino inversion was studied by gradually varying the improper dihedral C3′-P-N3′-H from 115° to 250°

in 15° increments. For the γ dihedral surfaces, constraints were introduced in other backbone dihedrals to keep them in the A-form (for the C3′-*endo* conformation) and B-form (for the C2′-*endo* conformation) conformations. The constraint values for these dihedrals were determined based on previously determined modal values of experimentally observed distributions of each dihedral in the A-DNA and B-DNA conformations (20,28,29). This approach has the obvious disadvantage that complete relaxation of the other dihedral degrees of freedom in the model compound is not allowed, however, it ensures sampling of the most interesting regions of conformation space and prevents complications in the specific dihedral surface being studied.

MD simulations were carried out on four oligonucleotide systems having the *Eco*RI recognition sequence CGCGAATTCGCG. The *Eco*RI or 'Dickerson–Drew dodecamer' sequence has been extensively studied using both theoretical and experimental techniques for regular DNA (30–36) as well as N3′-DNA backbones (13,14). The choice of this sequence allows for direct comparison of the present results with those previous studies. The four systems studied presently are: (i) RNA in the A-form with uracil replacing thymine; (ii) N3′-DNA in the B-form; (iii) N3′-DNA in the A-form X-ray crystal structure; and (iv) DNA in the B-form. Henceforth these will be referred to as ARNA, N3′BDNA, N3′ADNA and BDNA, respectively. Figure 1 illustrates the substitutions in the systems and the relevant torsional degrees of freedom. Simulations of the oligonucleotide systems were initiated by the oligonucleotide being overlaid with a pre-equilibrated solvent box consisting of water and sodium ions, which extended at least 7.0 Å beyond the DNA solute. All solvent molecules having a non-hydrogen atom within 1.8 Å of the DNA were deleted. Adjustment of the number of sodium ions was done to ensure electrostatic neutrality of the system by adding sodium ions at random positions in the box or deleting the sodium ions furthest from the DNA. Periodic boundary conditions were used in all subsequent calculations with the images generated using the CRYSTAL module (37). The system was minimized for 500 Adopted Basis Newton–Raphson (ABNR) steps with mass-weighted harmonic constraints of 2.0 kcal/mol/Å on the DNA atoms. The minimized system was then subjected to a 20 ps constant volume, isothermal (NVT) ensemble MD simulation keeping the same harmonic constraints in order to equilibrate the solvent around the DNA. The resulting system was minimized for 500 ABNR steps without any constraints and the final structure was used to initiate the production trajectories. Production MD simulations were performed for 2 ns in the isobaric, isothermal (NPT) ensemble (38) at 300 K with the Leap-Frog integrator. All calculations were performed using SHAKE (39) to constrain covalent bonds containing hydrogen, with an integration time step of 0.002 ps, and treating long-range electrostatic interactions using the Particle Mesh Ewald (PME) approach (40). PME calculations were performed using real space and Lennard–Jones (LJ) interaction cut-offs of 10 Å, with non-bond interaction lists maintained and heuristically updated out to 12 Å. The fast Fourier transform grid densities were set to ~1/Å using a fourth order smoothing spline. The screening parameter (κ) was set to 0.35. Analysis of DNA structural parameters was done using the FREEHELIX program (41) modified to read CHARMM-generated MD trajectories.

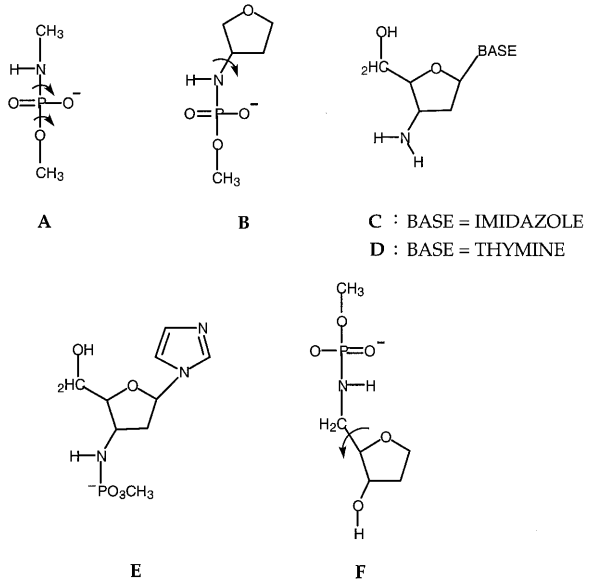

Figure 2. Model compounds representative of N3′-DNA used for parameterization of N3′-DNA. The curved arrows are indicative of the bond rotations studied as potential energy dihedral surfaces.

Except where explicitly stated, all analyses were performed on the last 1500 ps of the simulations, allowing for 500 ps of initial equilibration.

RESULTS AND DISCUSSION

Parameterization

The local conformational behavior of the N3′-H moiety was studied using *ab initio* calculations on the representative model compounds shown in Figure 2. The results of these calculations were used in parameterization of the N3′-DNA in the CHARMM force field for nucleic acids (20,21). The various criteria considered in the parameterization included reproduction of internal geometric parameters, such as bond length and angles, vibrational spectra, water interaction distances and energies, sugar pucker energies, dihedral and improper dihedral potential energy surfaces and experimental condensed phase structural properties. The parameterization involving the criteria intimately associated with dynamic properties observed in the MD simulations, like sugar pucker changes, local dihedral motions and N3′-H flexibility, are described in the following section. A detailed description of additional parameterization methods and results is reported in Supplementary Material.

Sugar pucker. A defining characteristic of the A-form structure at a local level is the north conformation of the sugar (42). The preference of the north sugar pucker in N3′-DNA has been suggested to be due to the reduced electronegativity of the N3′ substituent (11,13). The north sugar pucker preference of the N3′-DNA may, however, not be an intrinsic effect observable in the gas phase but a solvation effect only observable in the aqueous phase (15). It should be noted that the relationship between electronegativity of 3′ substituents and sugar pucker in DNA was suggested by an NMR study for thymine nucleoside analogs that was carried out in the aqueous phase

Table 1. *Ab initio* and CHARMM sugar pucker relative energies for model compounds **B**–**E**

	Conformation	Model compound			
		B	**C**	**D**	**E**
Ab initio					
	C2′-*endo*	0.00	0.11	1.90	0.00
	O4′-*endo*	1.75	4.42	4.41	4.08
	C3′-*endo*	0.87	0.00	0.00	0.78
CHARMM					
	C2′-*endo*	2.04	2.41	2.42	0.03
	O4′-*endo*	3.62	4.45	4.89	4.30
	C3′-*endo*	0.00	0.00	0.00	0.00

Level of theory MP2/6-31G* for neutral compounds, MP2/6–31+G* for anionic compounds, all energies in kcal/mol.

and not *in vacuo* (43). In the previous MD study using the Dickerson–Drew dodecamer, the parameters relating to sugar pucker for N3′-DNA had been adjusted to intrinsically favor the north conformation, a choice that was based on the thymine nucleoside NMR study mentioned above (11). It is possible that stabilization of the C3′-*endo* sugar pucker due to solvation changes may be masked by introducing an artificial intrinsic over-stabilization in the gas phase. The choice of sugar pucker parameters in this study was therefore made to reproduce, as best possible, the relative intrinsic energies of the sugar pucker in various representative model compounds calculated in the gas phase using high level quantum mechanics.

Table 1 shows a comparison between *ab initio* and CHARMM sugar pucker relative energies in the gas phase for the various model compounds. The inability to reproduce the energy differences quantitatively is due to the fact that subtle stereoelectronic effects cannot always be incorporated successfully for all conformations when using a simplified potential energy function. The emphasis was to obtain good agreement with the more complex model compounds (compounds **D** and **E**) and to sacrifice some accuracy in the smaller, less complex model compounds (compounds **B** and **C**). An overall bias favoring the north conformation is seen when the *ab initio* gas phase results are compared to the CHARMM gas phase results. While a large intrinsic bias for the C3′-*endo* conformation is to be avoided, a small bias in the force field for the north conformation is necessary since it is representative of the polarization effects of solvent on the DNA which are known to favor the north conformation, based on QM calculations that included aqueous solvation via a reaction field model (15); such solute polarization effects due to aqueous solvation cannot be incorporated explicitly in the CHARMM force field. The largest over-stabilization of the north conformation is ~2.3 kcal/mol seen for model compound **C** (2.41 versus 0.11 kcal/mol). The O4′-*endo* barrier heights could not be reproduced exactly, with the CHARMM energies being generally higher than the QM results. The largest deviation for the O4′-*endo* barrier height is for compound **B** (3.62 versus 1.75 kcal/mol). In compound **D**, representative of the thymine nucleoside used in the NMR study of the effect of electronegativity of 3′ substituents (43), the excess

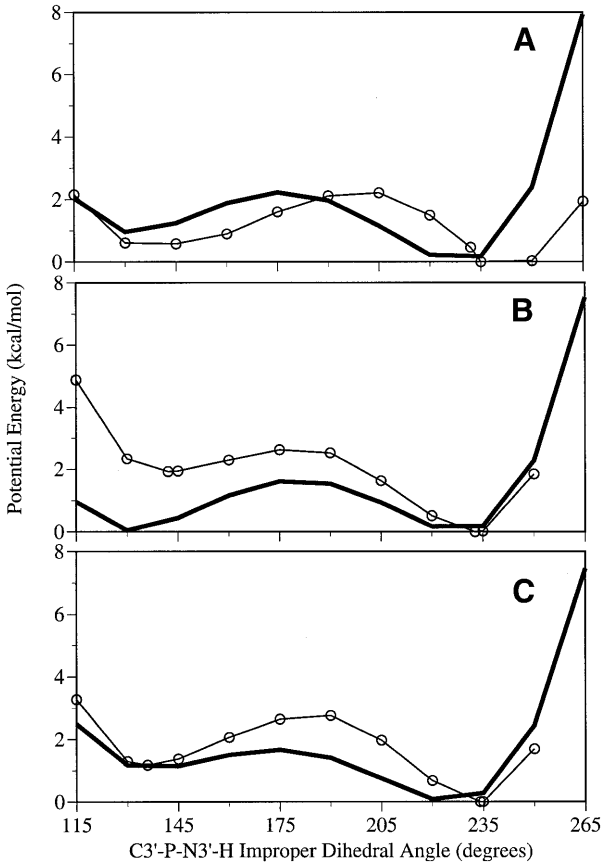

Figure 3. Comparison of CHARMM (bold line) and *ab initio* (line with open circles) MP2/6-31+G* inversion surfaces for the N3′-H moiety represented as C-P-N-H improper dihedral potential energy surfaces. (**A**) C-P-N-H surface for compound **A**; (**B**) C-P-N-H surface for compound **B**, south sugar conformation; (**C**) C-P-N-H surface for compound **B**, north sugar conformation.

stabilization of the north conformation is ~0.5 kcal/mol (2.42 versus 1.90 kcal/mol). In compound **E**, which best represents the sugar moiety in DNA, the excess stabilization of the north conformation is ~0.8 kcal/mol. As is evident, the parameters have been optimized such that the trend in gas phase sugar conformation energetics is reproduced overall, but most accurately reproduced in the compounds that best represent N3′-DNA.

N3′-H conformational properties. While the two possible orientations of the N3′-H moiety were considered in previous theoretical studies of the N3′-DNA backbone (10,11), interconversion between them was not discussed. The flexibility of the N3′-H moiety was studied in model compounds **A** and **B** using the C3′-P-N3′-H improper dihedral surface (Fig. 3A–C). This surface is an inversion surface of the N3′-H moiety and, therefore, involves orbital rehybridization (44). It is obvious that empirical force fields cannot explicitly treat these subtle electronic effects, however, it is possible to reproduce the overall inversion surface by using a combination of dihedral and improper dihedral parameter terms. The tetrahedral nature of the N3′-H moiety in the gas phase results in the presence of two minima in the inversion surface of the C-P-N-H improper dihedral at values of ~145° and ~230°, respectively. Figure 3A

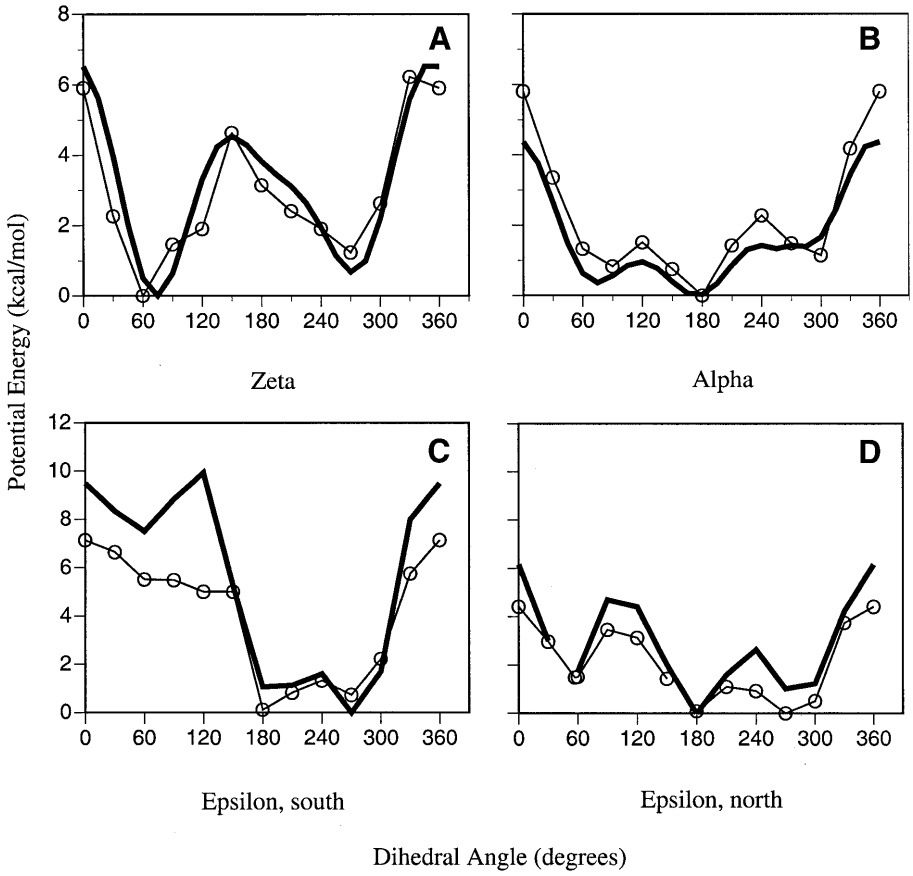

Figure 4. Comparison of CHARMM (bold line) and *ab initio* (line with open circles) HF/6-31+G* dihedral energy surfaces for dihedrals closely associated with the N3′-H substitution. (**A**) *z* dihedral in compound **A**; (**B**) α dihedral in compound **A**; (**C**) ε dihedral in compound **B**, south sugar conformation; (**D**) ε dihedral in compound **B**, north sugar conformation.

represents the inversion surface in model compound **A**, which is not complicated by the presence of the adjacent sugar. The inversion surfaces in model compound **B** for the C2′-*endo* (south) and C3′-*endo* (north) constrained conformations of the adjacent sugar are represented in Figure 3B and C, respectively. The energy barriers to interconversion between the two energy minima are low (<2 kcal/mol) in all three surfaces. In addition, the energy difference between the two minima themselves is also low (<2 kcal/mol). Both presence of the sugar moiety and its pucker conformation marginally affect the inversion surface, with the north conformation of the sugar resulting in lower energies for the overall surface. Presence of the adjacent sugar introduces an additional degree of freedom of the sugar pucker for the inversion surface. The compromise in this inversion surface parameterization was for model compound **B** in the south conformation, which shows lower CHARMM energies for the 115–160° region of the inversion surface (Fig. 3B). The parameters are adjusted to better reproduce the inversion surface in the absence of the sugar moiety (Fig. 3A) and in the presence of the north sugar moiety (Fig. 3C) for consistency with the observation that the north sugar conformation predominates in N3′-DNA duplexes in solution (9,14).

ε, α *and z dihedrals.* The N3′-H substitution is also likely to impact on the behavior of dihedrals adjacent to the substitution that are not directly linked to sugar pucker, namely the ε, *z* and α dihedrals. It is important to treat these dihedrals accurately to obtain a good model to describe N3′-DNA dynamics. Accordingly, the dihedral parameters for N3′-DNA were optimized to obtain good agreement with *ab initio* dihedral surfaces for representative model compounds. Figure 4A–D shows the dihedral surfaces for the α, *z* and ε dihedrals in model compounds **A** and **B**. Figure 4A and B represent the α and *z* dihedral surfaces in N3′-DNA studied in model compound **A**, which is the simplest model compound representing the phosphoramidate backbone. It can be seen that the developed force field adequately reproduces the *ab initio* results.

The ε dihedral surface presents more complications for parameterization since the dihedral surface is affected by the conformation of the sugar adjacent to it. In order to take this into account, the ε dihedral surface was studied for both the south and north constrained sugar conformations in model compound **B** (Fig. 4C and D, respectively). It is a difficult parameterization problem to have the same dihedral parameters reproduce two very different surfaces for the same dihedral. Our priority was first to reproduce the low energy conformations in both the surfaces accurately and then, if possible, to reproduce the high energy regions accurately for the north conformation, known to predominate in solution. As can be seen from Figure 4C and D, both these priorities have been fulfilled in reproducing the dihedral surface. The only sacrifice

Table 2. Average RMSD values for the non-hydrogen atoms for the entire 2 ns sampling period in the four MD simulation systems versus canonical A-form and B-form structure

System Starting structure	Canonical A-form	Canonical B-form
RNA (A-form)	2.96 (0.11)	6.60 (0.14)
N3′-DNA (B-form)	5.54 (0.09)	2.18 (0.03)
N3′-DNA (A-form)	2.77 (0.05)	4.86 (0.03)
DNA (B-form)	6.75 (0.06)	2.86 (0.04)

Standard errors in parentheses, RMSD values in Å.

made with respect to reproduction of the *ab initio* surface was for the high energy 0–150° region of the south ε dihedral surface (Fig. 4C), where the CHARMM energies are higher than the corresponding *ab initio* energies.

RNA, DNA and N3′-DNA dynamics

For the same sequence, the structural properties and melting temperatures of N3′-DNA show greater similarity to RNA than DNA (3,9). Structurally, like RNA, N3′-DNA assumes an A-form structure in low salt, in contrast to DNA, which assumes the B-form in a similar environment (9). N3′-DNA also demonstrates a higher melting temperature than DNA for the same sequence, again behaving similar to RNA (3). In this study, comparison with both RNA in the A-form and DNA in the B-form was made to understand the structural properties of N3′-DNA and how they contribute to the observed experimental properties.

Average root mean square deviations (RMSD) for the non-hydrogen atoms of the oligonucleotides in all four systems versus canonical A-DNA and B-DNA structures are shown in Table 2. As expected, the A-form of the RNA is seen to be preferred over the B-form. N3′ADNA starting from the A-form also prefers to stay closer to the canonical A-form. This is in contrast to what is observed for standard DNA of a shorter sequence simulated using a similar protocol and the same force field (21), which shows a transition from the A-form to the B-form within 500 ps. The surprising observation is that N3′BDNA starting from the B-form also stays closer to the B-form. Since the A-form is the more stable form for N3′-DNA in aqueous solution, it was expected that N3′BDNA should show a transition to the A-form. In fact, such a B→A transition was seen in the previous MD study of N3′-DNA using the AMBER force field (11). Regular DNA starting from the B-form also stays closer to the B-form, which is the expected result. These results seem to indicate a partial failure of the newly developed CHARMM force field parameters in treating the N3′-DNA moiety. Before the matter can be dismissed, however, it is essential to analyze the RMSD behavior of the N3′-DNA structures in the MD simulations starting from the A- and B-form DNA with respect to experimentally determined structures of N3′-DNA as opposed to the canonical forms of DNA.

Figure 5A and B shows the RMSD values for the simulated N3′-DNA oligonucleotides starting from the A- and B-forms, respectively, versus the experimental X-ray crystal structure (13) and the two NMR model structures (14). The RMSD time

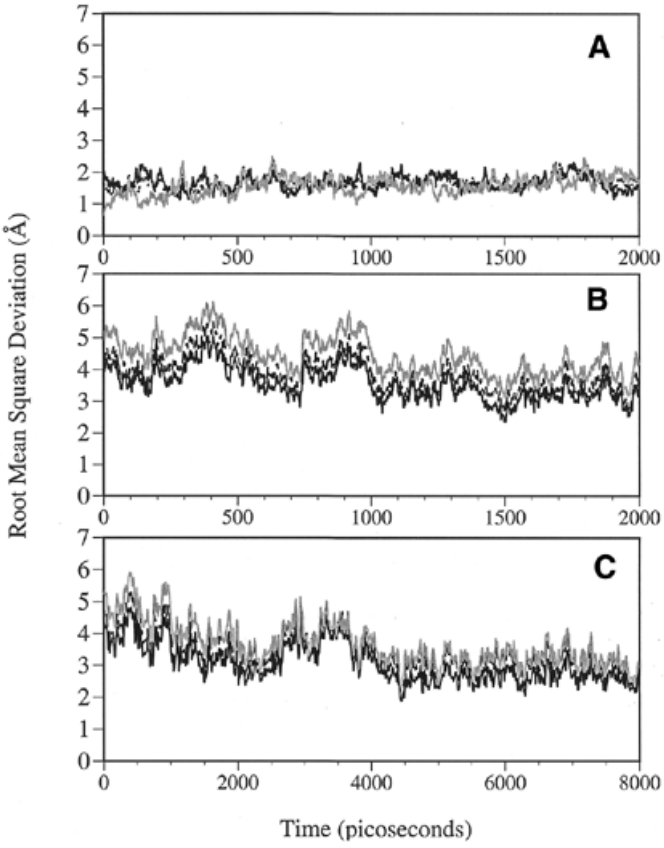

Figure 5. RMSD profiles of non-hydrogen atoms for the N3′-DNA simulation systems with respect to the experimentally determined N3′-DNA A-form structures. (**A**) A-form N3′-DNA; (**B**) B-form N3′-DNA; (**C**) B-form N3′-DNA extended to 8 ns simulation time. RMSD versus X-ray crystal structure, bold gray line; NMR model 1, bold black line; NMR model 2, dotted black line. Note that the two NMR models correspond to the two orientations of the N3′-H moiety.

series in Figure 5A shows that the N3′-DNA starting in the A-form stays very close to the experimental A-form structures throughout the 2 ns simulation (averages 1.58, 1.72 and 1.68 Å versus the X-ray, NMR-1 and NMR-2 models, respectively). Moreover, the RMSD from the experimental structures is smaller compared to the RMSD from canonical A-DNA (average 2.77 Å; see Table 2). This indicates clearly that the newly developed CHARMM force field for N3′-DNA not only maintains the A-form structure of the oligonucleotide over the B-form in aqueous solution, it can discriminate between the experimentally observed A-form structure and the canonical A-form structure. The RMSD time series in Figure 5B shows that N3′-DNA starting in the B-form does not show as much stability as the A-form starting structure. It can be seen that the N3′BDNA structure shows a trend towards the three experimental A-form structures with a drift of ~1 Å in RMSD over the 2 ns simulation (average RMSDs 4.45, 3.85 and 3.54 Å versus the X-ray, NMR-1 and NMR-2 models, respectively).

The simulation time of 2 ns is obviously not of sufficient duration to get the entire B→A transition, however, the correct trend is being observed. Subsequently, the N3BDNA simulation was extended to 8 ns to see if the transition could be observed in an extended sampling period. An analysis of the RMSD over the 8 ns simulation with respect to the experimental

structures (Fig. 5C) shows that the structure continues the trend of a slow transformation towards the experimental structures. Over the last 2 ns of the 8 ns simulation, the structure is equidistant from the canonical B-DNA and NMR model 2 structures. The average RMSD values over those last 2 ns are 2.69 Å from canonical B-DNA, 4.79 Å from canonical A-DNA, 3.05 Å from NMR model 1, 2.68 Å from NMR model 2 and 3.23 Å from the crystal structure. Thus, it appears that the present force field would ultimately yield the experimentally determined conformation if a long enough simulation was performed, further indicating the quality of the present force field for modeling N3′-phosphoramidate DNA.

The question that remains is whether a full transition from the B-form to the A-form should be observed within the timescale of 8 ns for N3′-DNA. A possible caveat of the previous study on N3′-DNA using the AMBER force field could be that the sugar pucker energetics were not tested explicitly using *ab initio* calculations to develop the sugar pucker parameters. Instead, the effect of reduced electronegativity on the sugar puckering of the N3′-substituent observed in the thymine nucleoside NMR study (43) was used to justify removal of the V2 torsion governing the relative energies of the south versus north conformations (11). This approach may lead to overstabilization of the north sugar pucker to a greater extent than is appropriate, which may be a possible explanation for the relatively quick B→A transition observed in that study. The other discrepancy is the dependence of the B→A transition of N3′-DNA on the initial conformation of the N3′-H moiety. The B→A transition was observed for the N3′-H 'in' starting orientation (C-P-N-H improper dihedral ~130°) but not observed for the N3′-H 'out' starting orientation (C-P-N-H improper dihedral ~240°) (11). *Ab initio* results on model compounds **A** and **B** suggest that the N3′-H moiety is flexible in both the gas phase and the aqueous phase (15). If the N3′-H moiety is flexible, it should exist in a fast equilibrium, as was observed in the present MD simulations (data not shown), and the global structural behavior of the N3′-DNA should not show such a strong dependence on the starting orientation of the N3′-H moiety.

It should be noted that A→B and B→A transitions in standard oligonucleotides have been studied extensively using MD simulations (17,21,45–49). The actual timescale of A→B and B→A transitions in short sequences of DNA remains, to the best of our knowledge, an unresolved issue due to lack of experimental corroboration.

Sugar pucker, C-P-N-H improper and local dihedral dynamics

Results in the previous section show that the overall structural behavior of the N3′-DNA in the present study agrees with experimental data. A careful scrutiny of the local behavior observed in our simulations of N3′-DNA in the A-form and B-form conformations is a necessary adjunct to understand whether the stabilization of the A-form structure is a simple matter of intrinsic stabilization of the north sugar pucker or whether other, more subtle factors linked to the N3′-H moiety are involved. The sugar pucker behavior of the N3′-oligonucleotides during the simulations is shown in Figure 6A and B in the form of histograms of the pseudorotation angle parameter, which is a good quantitative descriptor of the sugar pucker (50). The X-ray crystal structure pseudorotation angle distributions for A-form (solid gray line) and B-form (dotted gray line) DNA crystal structures (20) are also shown for comparative purposes. The sugars in the N3′ADNA simulation show a tendency to remain in the north conformation (Fig. 6A). This shows that the north conformation is stable for solvated N3′-DNA sugars. The sugars in the N3′-DNA simulation starting from the B-form structure show a significant population of north sugar puckers. Thus, there is a distinct tendency to convert from the south sugar pucker (characteristic of the B-form) to the north sugar pucker (characteristic of the A-form) (Fig. 6B).

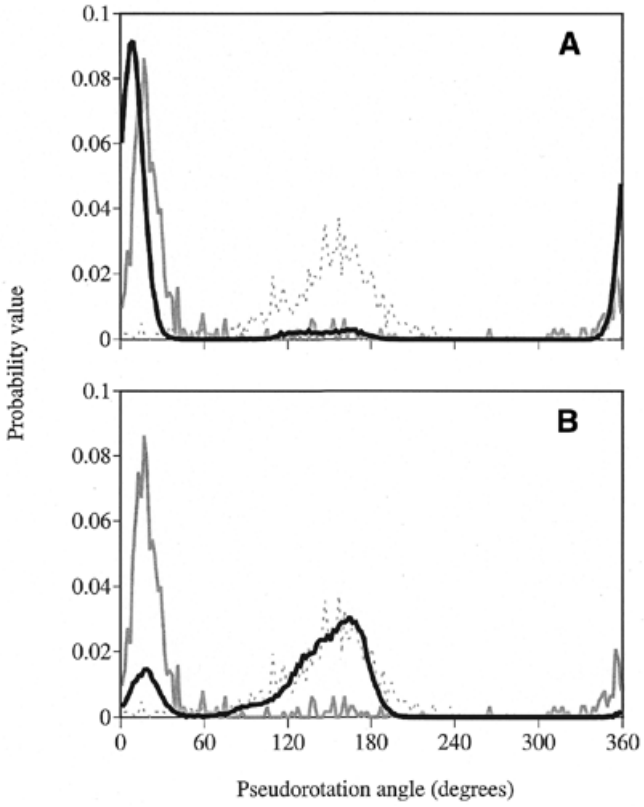

Figure 6. Sugar pucker conformations represented as pseudorotation angle probability distributions from the last 1500 ps of simulation. (**A**) A-form N3′-DNA simulation; (**B**) B-form N3′-DNA simulation. Bold gray line, X-ray crystal structure sugar pucker distribution of A-form DNA structures; dotted gray line, X-ray crystal structure sugar pucker distribution of B-form DNA structures.

The data presented in Figure 6 was obtained by grouping all the sugars in the oligonucleotide together, so there are two possible explanations for this behavior. First, all the sugars in the B-form N3′-DNA exist in an equilibrium between the south and north conformations or, second, some of the sugars have made a transition to the north form while some other sugars remain in the starting south form. Examination of all the sugar pucker time series (data not shown) showed that the latter is the case. Some of the nucleotides of the dodecamer that make transitions to the north sugar pucker conformations are Cyt3, Ade5, Thy8 and Cyt9 of strand 1 and Cyt3, Cyt9 and Cyt11 of strand 2. These results are consistent with the RMSD results in Figure 5B, which indicate that the N3′-DNA originating in the B-form is in the process of making a transition to the A-form.

It was shown in an earlier study that model compounds **A** and **B** showed a change in preference between the two

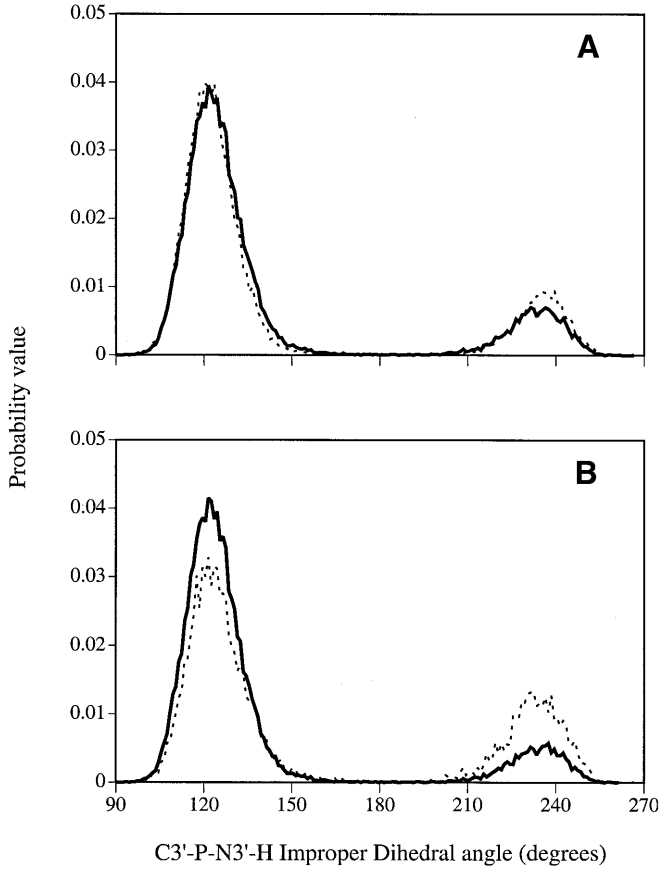

Figure 7. The inversion equilibrium for the N3′-H moiety represented as C-P-N-H improper dihedral probability distribution from the last 1500 ps of simulation. (**A**) Comparison between experimental A-form and B-form N3′-DNA simulations. Experimental A-form N3′-DNA, dotted line; B-form N3′-DNA, bold line. (**B**) Comparison between north and south conformation sugars in the B-form N3′-DNA simulation. Sugars making transition to north conformation, dotted line; sugars remaining in south conformation, bold line.

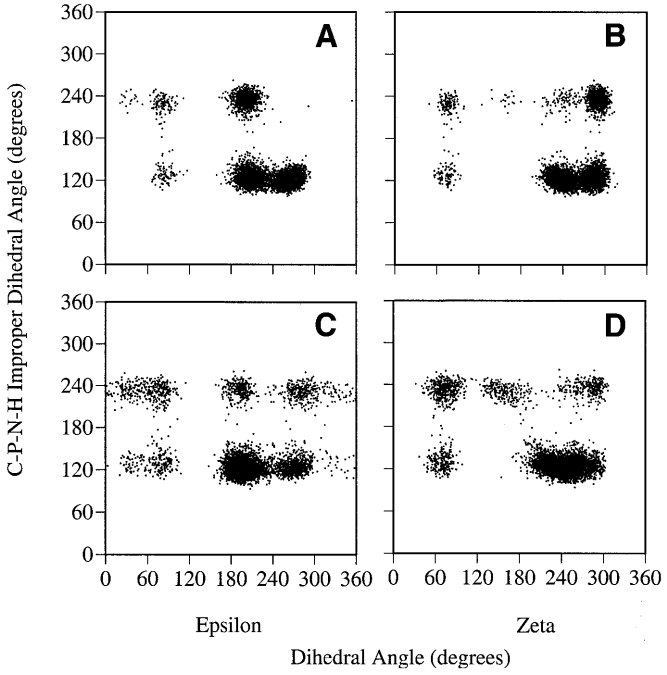

Figure 8. Correlation plots for ε and ζ dihedrals versus the C-P-N-H dihedral for the last 1500 ps of simulation. (**A**) A-form N3′-DNA, ε versus C-P-N-H; (**B**) A-form N3′-DNA, ζ versus C-P-N-H; (**C**) B-form N3′-DNA, ε versus C-P-N-H; (**D**) B-form N3′-DNA, ζ versus C-P-N-H.

minimum energy N3′-H orientations when aqueous solvation was included using an implicit model, while the flexibility of the N3′-H was maintained in both phases (15). Based on these results, our parameterization focused on properly representing the flexibility of the N3′-H moiety in the gas phase. It is of great interest, therefore, to observe the nature of this flexibility in N3′-DNA in the explicit solvent MD simulations. Figure 7A shows the probability distribution of the C3′-P-N3′-H dihedral in the N3′-DNA A-form and B-form simulations. The N3′-H moiety exists in an equilibrium between the two minima on the inversion surface, with the 130° state more populated. This indicates that there is no single 'correct' orientation of the N3′-H moiety as previously suggested (11,13). Rather, both the minimum energy states exist in an equilibrium. Even more interesting is the observation that the most populated N3′-H inversion state (C-P-N-H improper ~130°) is not the orientation that is more stable in the gas phase (C-P-N-H improper ~230°; Fig. 3). The preferred orientation seen here is, however, the same one predicted by both the X-ray and NMR structural studies (13,14). Thus, the present calculations are able to reproduce the change in preference of the N3′-H orientation in going from the gas phase to the aqueous phase by properly treating the energetic balance between the two states.

Figure 7A shows the probability distributions for all the N3′-H moieties in the experimentally observed A-form (dotted line) and the B-form (bold line) N3′-DNA simulations. There are marginal differences detectable for the two distributions. In the A-form simulations, the N3′-H moieties populate the state with the C-P-N-H dihedral value of ~230° slightly more than in the B-form simulations. To clarify the differences between the flexibility behavior of the N3′-H moiety for south versus north sugars, the N3′-H moieties from the B-form starting simulation were separated into two groups. The first group contained the sugars that had made the transition to the north conformation (see above) and the second group contained the sugars that had not made this transition. This separation enabled us to compare, with greater precision, the effect of south and north unconstrained sugar conformations on N3′-H flexibility. As seen in Figure 7B, the 230° C-P-N-H dihedral state is populated to a greater extent for the north sugars (dotted line) than the south sugars (bold line). This is consistent with the observation in Figure 7A, indicating that the north sugar conformation may be associated with a greater possibility of transition to the C-P-N-H 230° orientation. This may be an artifact of the inability to reproduce the N3′-H inversion surface entirely for the constrained south conformation (Fig. 3B) or a real effect of enhanced flexibility of the N3′-H moiety adjacent to an unconstrained north sugar in N3′-DNA.

The N3′-H moiety is expected to have an impact on the local backbone dihedrals directly adjacent to the substitution. Scatter plots between the ε and C-P-N-H dihedrals (Fig. 8A and C) and between the *z* and C-P-N-H dihedrals (Fig. 8B and D) are used to study their mutual relationship. Figure 8A and B represents the A-form N3′-DNA system and Figure 8C and D represents the B-form N3′-DNA system. The C-P-N-H

improper dihedral is plotted on the *y*-axis. Comparison of Figure 8A and C shows that the ε dihedral tends to populate a much wider range for the B-form structure than the A-form structure. This is a possible indication of the structural instability of this dihedral when a south conformation sugar is adjacent to it. Population of ε around 0–60° and 300–360° is greater for the B-form structure. The population of the region around 0–60° is surprising for the B-form structure because this region is of high energy for the south sugar conformation (Fig. 4C). The explanation for this observation is that population of this region is mostly due to the sugars that made the transition to the north conformation (data not shown), for which this region has a local minimum (Fig. 4D). Another interesting feature of ε observed for the A-form structure is the lack of sampling of the region around C-P-N-H ~240° and ε ~270° (Fig. 8A). This lack of sampling indicates that the N3′-H orientation with the C-P-N-H dihedral ~130° allows the ε dihedral to populate regions close to 200° as well as 270°. The N3′-H orientation with C-P-N-H dihedral ~240°, on the other hand, restricts the ε dihedral to the 200° region alone. Thus, with the C-P-N-H improper in the vicinity of 130° greater local relaxation of ε is allowed. This may contribute to the prevalence of C-P-N-H improper being ~130° versus ~240°, in spite of the lower intrinsic gas phase energy at 240° (Fig. 3C).

For the *z* dihedral the B-form structure (Fig. 8D) more evenly samples the range of *z* values as compared to the A-form structure (Fig. 8B), with the most noticeable difference being a greater population of the 120–180° region. The population of this region is almost exclusively linked to the C-P-N-H improper being ~240°. This region is neither a minimum in the dihedral gas phase surface (Fig. 4A) nor a region normally populated in crystal structures of DNA (~262° for B-DNA, ~287° for A-DNA) (20). The population of these high energy states in the B-form structure simulation may be a consequence of this structure trying to make a transition to the A-form. Increased sampling of the 200–300° region of *z* when the C-P-N-H improper is ~130° versus 240° is also apparent.

Thus, a structural equilibrium between primarily two states is seen for both the ε and *z* dihedrals of N3′ADNA. This is in contrast to duplex DNA, where ε is found only in the region of 180–300° and where *z* is only found in the region of 150–320° (21). Such local flexibility in the backbone dihedrals may directly reduce the entropic penalty of duplex formation in N3′-DNA contributing to its greater stability as compared to DNA. In addition, such flexibility may indirectly reduce the entropic penalty by allowing some reorganization of water molecules hydrogen bonded to the N3′-DNA.

Hydration

Hydration around the N3′-phosphoramidate backbone is seen to be enhanced in the crystal structure as compared to the corresponding DNA phosphodiester backbone (13). A previous theoretical study on N3′- and N5′-substituted oligonucleotides postulated that the differential hydration around the N3′-H moiety could be a contributing factor to the enhanced duplex stability and unusual structural properties of N3′-DNA (10). Table 3 shows hydration numbers for the four simulation systems around the N3′, O3′ and O2′ atoms. The first solvation shell includes all water oxygens within 3.5 Å of the atom, while the second solvation shell includes all waters within 5.5 Å of the specified atom. The choice of these cut-off distances was made based on the location of peaks representative of these solvation shells in the N3′-water oxygen radial distribution functions (not shown). It is clear that the hydration around the N3′ atom of N3′-DNA is increased as compared to the corresponding O3′ atom of regular B-form DNA. As previously postulated, this could be one of the important factors contributing to the preference for the A-form structure of N3′-DNA (10). Our previous *ab initio* results (15) indicate that the north pucker preference of the N3′-DNA sugars is an aqueous phase effect rather than an intrinsic gas phase effect. In this context, increased hydration around the N3′ atom is likely to better hydrate and consequently stabilize the north sugar pucker. It is also clear that the enhancement in hydration by the N3′ atom is not restricted to the first solvation shell but extends beyond it. This is consistent with the crystal structure study showing that waters not directly bound to the N3′ atom are also immobilized on the N3′-phosphoramidate backbone (13).

Table 3. Hydration numbers for the four MD simulation systems for the first two solvation shells around N3′ or O3′ or O2′ primary atoms

Structure	Atom type	(O_{wat} within 3.5 Å)	(O_{wat} within 5.5 Å)
RNA (A-form)	O3′	1.24 (0.01)	12.99 (0.05)
	O2′	2.52 (0.02)	11.69 (0.08)
N3′-DNA (B-form)	N3′	1.29 (0.01)	13.27 (0.08)
N3′-DNA (A-form)	N3′	1.32 (0.01)	13.05 (0.02)
DNA (B-form)	O3′	1.06 (0.03)	12.28 (0.20)

Standard errors in parentheses, O_{wat} refers to water oxygens.

Interestingly, for the A-form N3′-DNA simulation, the hydration around the N3′ atom is slightly better than the corresponding O3′ atom of the A-form RNA simulation (Table 3). The local hydration around the RNA O2′ atom, which is part of a hydrogen bond donor group like the N3′ atom, is better in the first solvation shell but is not as high when the second solvation shell is also considered (Table 3). This is probably due to the location of the RNA O2′ atom at the edge of the major groove that makes it relatively less solvent accessible compared to the N3′ atom located on the backbone. Thermodynamic studies on RNA and DNA show that the greater duplex stability of RNA as compared to DNA is due to greater enthalpic stabilization upon duplex formation (51). This greater enthalpic stabilization is also accompanied by an increased entropic penalty (51). These effects have been explained previously by the greater hydration around RNA as compared to DNA; according to this hypothesis, waters bound to the RNA backbone provide greater enthalpic stabilization but result in a greater entropic penalty because their motion is hindered. Since the thermodynamic properties of the duplex RNA or DNA are dependent upon differences between the duplex state and the unfolded, single-stranded state, such a comparison between hydration of RNA and DNA duplexes implicitly assumes that the hydration in the structurally disordered single-stranded state is similar for RNA and DNA. N3′-DNA is shown to have similar thermodynamic properties but with an increased enthalpic stabilization and entropic penalty as compared to RNA (13). These properties of N3′-DNA have not been attributed to greater hydration, since

crystallographic studies show the first solvent shell hydration of N3′-DNA to be similar to RNA. Rather, the greater enthalpic stabilization of N3′-DNA as compared to RNA was explained in terms of cation/anion condensation near the oligonucleotide and the anomeric effect (13). Our simulation data indicates, however, that hydration around the N3′-DNA backbone may be stabilized to a greater extent than the RNA backbone. While the hydration differences are small in the first solvation shell, they can be seen more clearly when the second solvation shell is also considered. This may explain why significant differences are not observed in crystallographic studies since only a few ordered water molecules typically belonging to the first solvation shell can be resolved (52). Assuming that the single-stranded structures of RNA and N3′-DNA have similar hydration, the greater enthalpic stabilization and greater entropic penalty may both be explained based on hydration differences of the backbone, consistent with previous work (51). It should be noted that the assumption that the single-stranded structures of RNA, DNA and N3′-DNA have similar hydration characteristics is debatable but difficult to test by simulation due to the conformational disorder in the single-stranded state. Using this assumption, however, differences in atomic level hydration properties of the duplex states can provide a consistent explanation of the greater observed duplex stability of N3′-DNA as compared to RNA as well as DNA (3).

N5′-phosphoramidate backbone conformational properties

An earlier theoretical study attributed the differences between the thermodynamic properties of N3′- and N5′-phosphoramidate analogs to the differences in their hydration properties (10). The effect that this substitution has on the intrinsic conformational properties of the DNA backbone has not been studied. The N5′-H moiety is expected to show flexibility similar to the N3′-H moiety but the alternative location of the N5′-H moiety in the backbone means the effect of this flexibility on the DNA backbone may be different. Recently, we demonstrated that changes in the intrinsic properties of the γ dihedral caused by conformationally constrained sugars in a single nucleotide are linked to differences in the flipping properties of the DNA backbone (53). If the γ dihedral along the entire DNA backbone is perturbed then it may be postulated that the overall thermodynamic properties, such as the melting temperature and hybridization efficiency, may be significantly affected. The N5′-H substitution is in close proximity to the γ dihedral. The effect that this substitution has on the conformational properties of the γ dihedral was, therefore, studied using model compound **F** (Fig. 2).

The γ dihedral energy surfaces for compound **F** are presented in Figure 9. Both C2′-*endo* and C3′-*endo* sugar conformations were studied since the sugar conformation is known to affect the properties of the γ dihedral (28,53). As previously observed, the C3′-*endo* sugar conformation causes the *gauche*$^-$ conformation of the γ dihedral (~300°) to be of a higher energy than the *gauche*$^+$ conformation (~60°) (53). On the other hand, for the C2′-*endo* conformation, it is observed that the *gauche*$^-$ conformation of γ is of lower energy than the *gauche*$^+$ conformation. For the C2′-*endo* conformation in regular DNA, the *gauche*$^-$ conformation is of approximately the same energy as the *gauche*$^+$ conformation, while for the C3′-*endo* conformation the *gauche*$^-$ conformation has a higher energy than the *gauche*$^+$ conformation (28,53). It should also be noted that in experimental structures of both A- and B-form duplex DNA, the *gauche*$^-$ conformation is populated to a very small extent, if at all, and the *gauche*$^+$ conformation dominates (28). This suggests that the *gauche*$^-$ state, while not energetically prohibited at a local level, is not favored in the context of duplex DNA. Based on the γ dihedral surfaces presented in Figure 9, it may be postulated that the decreased stability of the *gauche*$^+$ state of γ in the C2′-*endo* conformation of the N5′-substituted deoxyribose sugar contributes to the lack of stability of duplex N5′-DNA. MD studies of N5′-phosphoramidate DNA analogs that incorporate these intrinsic properties in the atomic model description are needed to assess the effect of this perturbation of the γ dihedral on the overall dynamic properties of N5′-phosphoramidate analogs.

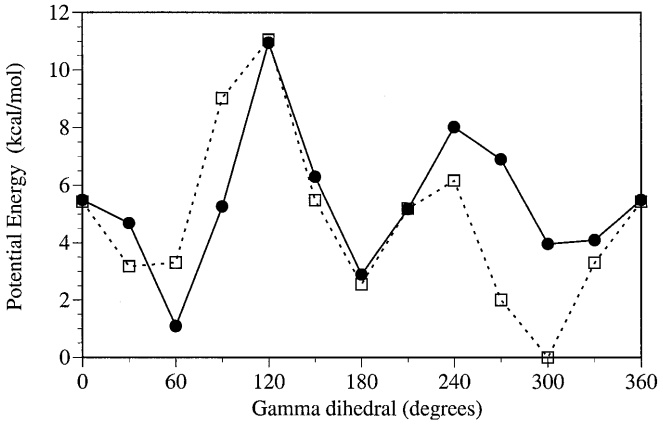

Figure 9. γ dihedral surface for the C2′-*endo* (dotted line, blank squares) and C3′-*endo* conformations (bold line, filled circles) of model compound **F** (Fig. 2) representing the N5′-phosphoramidate DNA backbone.

CONCLUSION

The present study sheds light on an aspect of the N3′-H moiety in N3′-DNA that has been overlooked in previous studies. The N3′-H moiety in N3′-DNA is found to be flexible and exists in an equilibrium between two possible inversion states associated with the C-P-N-H improper dihedral. This equilibrium is dynamic and is possibly affected by hydration of the N3′-DNA. Through its flexibility, the N3′-H moiety distinctly alters the dynamic properties of the adjacent sugar and backbone dihedrals. The N3′-H substitution is also seen to influence hydration of the backbone, a property which may be critical in determining the thermodynamic properties of N3′-DNA. The combination of these intrinsic and environmental changes are postulated to contribute to stabilizing the overall A-form structure of N3′-DNA and improving duplex stability in aqueous solution. A specific perturbation caused by the N5′-H substitution in the γ dihedral is observed using QM calculations on a model compound and postulated to possibly contribute to changes in the observed thermodynamic properties for N5′-phosphoramidate DNA. Further studies are, however, needed to understand the effect of this intrinsic change on the overall dynamic properties of the N5′-DNA backbone.

SUPPLEMENTARY MATERIAL

Supplementary Material is available at NAR Online.

ACKNOWLEDGEMENTS

This work was supported by NIH grant GM-51501 and computational support from the National Partnership for Advanced Computational Infrastructure, DOD ASC Major Shared Resource Computing and the Pittsburgh Supercomputing Center.

REFERENCES

1. Myers,K.J. and Dean,N.M. (2000) Sensible use of antisense: how to use oligonucleotides as research tools. *Trends Pharm. Sci.*, **21**, 19–23.
2. Escude,C., Giovannangeli,C., Sun,J.-S., Lloyd,D.H., Chen,J.-K., Gryaznov,S.M., Garestier,T. and Helene,C. (1996) Stable triple helices formed by oligonucleotide N3′-P5′ phosphoramidates inhibit transcription elongation. *Proc. Natl Acad. Sci. USA*, **93**, 4365–4369.
3. Gryaznov,S.M., Lloyd,D.H., Chen,J.-K., Schultz,R.G., DeDionisio,L.A., Ratmeyer,L. and Wilson,W.D. (1995) Oligonucleotide N3′-P5′ phosphoramidates. *Proc. Natl Acad. Sci. USA*, **92**, 5798–5802.
4. Boulme,F., Freund,F., Moreau,S., Nielsen,P.E., Gryaznov,S., Toulme,J.-J. and Litvak,S. (1998) Modified (PNA, 2′-*O*-methyl and phosphoramidate) anti-TAR antisense oligonucleotides as strong and specific inhibitors of *in vitro* HIV-1 reverse transcription. *Nucleic Acids Res.*, **26**, 5492–5500.
5. Rigl,T., Lloyd,D.H., Tsou,D.S., Gryaznov,S.M. and Wilson,W.D. (1997) Structural RNA mimetics: N3′-P5′ phosphoramidate DNA analogs of HIV-1 RRE and TAR RNA form A-type helices that bind specifically to Rev and Tat-related peptides. *Biochemistry*, **36**, 650–659.
6. Testa,S.M., Gryaznov,S.M. and Turner,D.H. (1999) *In vitro* suicide inhibition of self-splicing of a group I intron from *Pneumocystis carinii* by an N3′-P5′ phosphoramidate hexanucleotide. *Proc. Natl Acad. Sci. USA*, **96**, 2734–2739.
7. Testa,S.M., Gryaznov,S.M. and Turner,D.H. (1998) Antisense binding enhanced by tertiary interactions: binding of phosphorothioate and N3′-P5′ phosphoramidate hexanucleotides to the catalytic core of a Group I ribozyme from the mammalian pathogen *Pneumocystis carinii*. *Biochemistry*, **37**, 9379–9385.
8. Skorski,T., Perotti,D., Nieborowska-Skorska,M., Gryaznov,S. and Calabretta,B. (1997) Antileukemia effect of c-*myc* N3′-P5′ phosphoramidate antisense oligonucleotides *in vivo*. *Proc. Natl Acad. Sci. USA*, **94**, 3966–3971.
9. Ding,D., Gryaznov,S.M., Lloyd,D.H., Chandrasekaran,S., Yao,S., Ratmeyer,L., Pan,Y. and Wilson,W.D. (1996) An oligonucleotide N3′-P5′ phosphoramidate duplex forms an A-type helix in solution. *Nucleic Acids Res.*, **24**, 354–360.
10. Barsky,D., Colvin,M.E., Zon,G. and Gryaznov,S.M. (1997) Hydration effects on the duplex stability of phosphoramidate DNA-RNA oligomers. *Nucleic Acids Res.*, **25**, 830–835.
11. Cieplak,P., Cheatham,T.E. and Kollman,P.A. (1997) Molecular dynamics simulations find that 3′ phosphoramidate modified duplexes undergo a B to A transition and normal DNA duplexes an A to B transition. *J. Am. Chem. Soc.*, **119**, 6722–6730.
12. Srinivasan,J., Cheatham,I.,T.E., Ceiplak,P., Kollman,P.A. and Case,D.A. (1998) Continuum solvent studies of the stability of DNA, RNA and phosphoramidate-DNA helices. *J. Am. Chem. Soc.*, **120**, 9401–9409.
13. Tereshko,V., Gryaznov,S. and Egli,M. (1998) Consequences of replacing the DNA 3′-oxygen by an amino group: high-resolution crystal structure of a fully modified N3′-P5′ phosphoramidate DNA dodecamer duplex. *J. Am. Chem. Soc.*, **120**, 269–283.
14. Ding,D., Gryaznov,S.M. and Wilson,W.D. (1998) NMR solution structure of the N3′-P5′ phosphoramidate duplex d(CGCGAATTCGCG) by iterative relaxation matrix approach. *Biochemistry*, **37**, 12082–12093.
15. Banavali,N.K. and MacKerell,A.D.Jr (2001) Reevaluation of stereoelectronic contributions to the phosphodiester and N3′-phosphoramidate moieties in nucleic acids. Submitted for publication.
16. Cramer,C.J. and Truhlar,D.G. (1992) Anomeric and reverse anomeric effects in the gas phase and aqueous solution. *J. Org. Chem.*, **57**, 7034.
17. Cheatham,T.E. and Kollman,P.A. (1996) Observation of the A DNA to B DNA transition during unrestrained molecular dynamics simulations in aqueous solution. *J. Mol. Biol.*, **259**, 434–444.
18. Brooks,B.R., Bruccoleri,R.E., Olafson,B.D., States,D.J., Swaminathan,S. and Karplus,M. (1983) CHARMM: a program for macromolecular energy, minimization and dynamics calculations. *J. Comput. Chem.*, **4**, 187–217.
19. MacKerell,A.D.Jr, Brooks,B., Brooks,C.L., Nilsson,L., Roux,B., Won,Y. and Karplus,M. (1998) In Schleyer,P.v.R. (ed.) *Encyclopedia of Computational Chemistry*. Wiley, New York, NY.
20. Foloppe,N. and MacKerell,A.D.Jr (2000) All-atom empirical force field for nucleic acids: 1) Parameter optimization based on small molecule and condensed phase macromolecular target data. *J. Comp. Chem.*, **21**, 86–104.
21. MacKerell,A.D.Jr and Banavali,N. (2000) All-atom empirical force field for nucleic acids: 2) Application to molecular dynamics simulations of DNA and RNA in solution. *J. Comp. Chem.*, **21**, 105–120.
22. Jorgensen,W.L., Chandrasekhar,J., Madura,J.D., Impey,R.W. and Klein,M.L. (1983) Comparison of simple potential functions for simulating liquid water. *J. Chem. Phys.*, **79**, 926–935.
23. Reiher,W.E. (1985) Theoretical studies of hydrogen bonding, PhD thesis, Harvard University, Cambridge, MA.
24. Beglov,D. and Roux,B. (1994) Finite representation of an infinite bulk system: solvent boundary potential for computer simulations. *J. Chem. Phys.*, **100**, 9050–9063.
25. Frisch,M.J., Trucks,G.W., Schlegel,H.B., Gill,P.M.W., Johnson,B.G., Robb,M.A., Cheeseman,J.R., Raghavachari,K., Al-Laham,M.A., Zakrzewski,V.G., Ortiz,J.V., Foresman,J.B., Cioslowski,J., Stefanov,B.B., Nanayakkara,A., Challacombe,M., Peng,C.Y., Ayala,P.Y., Chen,W., Wong,M.W., Andres,J.L., Replogle,E.S., Gomperts,R., Martin,R.L., Fox,D.J., Binkley,J.S., Defrees,D.J., Baker,J., Stewart,J.J.P., Head-Gordon,M., Gonzalez,C. and Pople,J.A. (1996) *GAUSSIAN94, Revision C*, 3rd Edn. Gaussian Inc., Pittsburgh, PA.
26. Frisch,M.J., Trucks,G.W., Schlegel,H.B., Scuseria,G.E., Robb,M.A., Cheeseman,J.R., Zakrzewski,V.G., Montgomery,J.A.Jr, Stratmann,R.E., Burant,J.C., Dapprich,S., Millam,J.M., Daniels,A.D., Kudin,K.N., Strain,M.C., Farkas,O., Tomasi,J., Barone,V., Cossi,M., Cammi,R., Mennucci,B., Pomelli,C., Adamo,C., Clifford,S., Ochterski,J., Petersson,G.A., Ayala,P.Y., Cui,Q., Morokuma,K., Malick,D.K., Rabuck,A.D., Raghavachari,K., Foresman,J.B., Cioslowski,J., Ortiz,J.V., Stefanov,B.B., Liu,G., Liashenko,A., Piskorz,P., Komaromi,I., Gomperts,R., Martin,R.L., Fox,D.J., Keith,T., Al-Laham,M.A., Peng,C.Y., Nanayakkara,A., Gonzalez,C., Challacombe,M., Gill,P.M.W., Johnson,B., Chen,W., Wong,M.W., Andres,J.L., Gonzalez,C., Head-Gordon,M., Replogle,E.S. and Pople,J.A. (1998) *GAUSSIAN98, Revision A*, 6th Edn. Gaussian Inc., Pittsburgh, PA.
27. Foloppe,N. and MacKerell,A.D.Jr (1998) Conformational properties of the deoxyribose and ribose moieties of nucleic acids: a quantum mechanical study. *J. Phys. Chem. B*, **102**, 6669–6678.
28. Foloppe,N. and MacKerell,A.D.Jr (1999) Intrinsic conformational properties of deoxyribonucleosides: role for cytosine in the equilibrium between the A, B and Z forms of DNA. *Biophys. J.*, **76**, 3206–3218.
29. Foloppe,N. and MacKerell,A.D.Jr (1999) Contribution of the phosphodiester backbone and glycosyl linkage intrinsic torsional energetics to DNA structure and dynamics. *J. Phys. Chem. B*, **103**, 10955–10964.
30. Young,M.A., Ravishanker,G. and Beveridge,D.L. (1997) A 5-nanosecond molecular dynamics trajectory for B-DNA: analysis of structure, motions and solvation. *Biophys. J.*, **73**, 2313–2336.
31. Minasov,G., Tereshko,V. and Egli,M. (1999) Atomic-resolution crystal structures of B-DNA reveal specific influences of divalent metal ions on conformation and packing. *J. Mol. Biol.*, **291**, 83–99.
32. Shui,X., McFail-Isom,L., Hu,G.G. and Williams,L.D. (1998) The B-DNA dodecamer at high resolution reveals a spine of water on sodium. *Biochemistry*, **37**, 8341–8355.
33. Denisov,A.Y., Zamaratski,E.V., Maltseva,T.V., Sandstrom,A., Bekiroglu,S., Altmann,K.H., Egli,M. and Chattopadhyaya,J. (1998) The solution conformation of a carbocyclic analog of the Dickerson-Drew dodecamer: comparison with its own X-ray structure and that of the NMR structure of the native counterpart. *J. Biomol. Struct. Dyn.*, **16**, 547–568.
34. Patel,D.J., Kozlowski,S.A. and Bhatt,R. (1983) Sequence dependence of base-pair stacking in right-handed DNA in solution: proton Nuclear Overhauser Effect NMR measurements. *Proc. Natl Acad. Sci. USA*, **80**, 3908–3912.

35. Drew,H.R., Wing,R.M., Takano,T., Broka,C., Tanaka,S., Itakura,K. and Dickerson,R.S. (1981) Structure of a B-DNA dodecamer: conformation and dynamics. *Proc. Natl Acad. Sci. USA*, **78**, 2179–2183.
36. Drew,H.R. and Dickerson,R.E. (1981) Structure of a B-DNA dodecamer III. Geometry of hydration. *J. Mol. Biol.*, **151**, 535–556.
37. Field,M.J. and Karplus,M. (1992) Harvard University, Cambridge, MA.
38. Feller,S.E., Zhang,Y., Pastor,R.W. and Brooks,R.W. (1995) Constant pressure molecular dynamics simulation: the Langevin Piston Method. *J. Chem. Phys.*, **103**, 4613–4621.
39. Ryckaert,J.P., Ciccotti,G. and Berendsen,H.J.C. (1977) *J. Comput. Phys.*, **23**, 327–341.
40. Darden,T., York,D. and Pederson,L. (1993) Particle mesh Ewald: an N.log(N) method for ewald sums in large systems. *J. Chem. Phys.*, **98**, 10089–10092.
41. Dickerson,R.E. (1998) DNA bending: the prevalence of kinkiness and the virtues of normality. *Nucleic Acids Res.*, **26**, 1906–1926.
42. Saenger,W. (1984) *Principles of Nucleic Acid Structure*. Springer-Verlag, New York, NY.
43. Thibadeau,C.J.P., Garg,N., Papchikin,A. and Chattopadhyaya,J. (1994) How does the electronegativity of the substituent dictate the strength of the gauche effect? *J. Am. Chem. Soc.*, **116**, 4038–4043.
44. Pophristic,V., Goodman,L. and Guchhait,N. (1997) Role of lone-pairs in internal rotation barriers. *J. Phys. Chem. A*, **101**, 4290–4297.
45. Cheatham,I.T.E. and Kollman,P.A. (1997) Molecular dynamics simulations highlight the structural differences among DNA:DNA, RNA:RNA and DNA:RNA hybrid duplexes. *J. Am. Chem. Soc.*, **119**, 4805–4825.
46. MacKerell,J.A.D. (1998) In Leontis,N.B. and SantaLucia,J.J. (eds) *Molecular Modeling of Nucleic Acids*. American Chemical Society, Washington, DC, Vol. 682, pp. 304–311.
47. Cheatham,I.T.E. and Kollman,P.A. (1997) Spontaneous B-DNA to A-DNA transitions observed in the molecular dynamics simulations of d[ACCCGCGGGT]$_2$ in the presence of hexamminecobalt(III). *Structure*, **5**, 1297–1311.
48. Cheatham,I.T.E., Crowley,M.F., Fox,T. and Kollman,P.A. (1997) A molecular level picture of the stabilization of A-DNA in mixed ethanol-water solutions. *Proc. Natl Acad. Sci. USA*, **94**, 9626–9630.
49. Langley,D. (1998) Molecular dynamics simulations of environment and sequence dependent DNA conformations: the development of the BMS nucleic acid force field and comparison with experimental results. *J. Biomol. Struct. Dyn.*, **3**, 487–509.
50. Altona,C. and Sundaralingam,M. (1972) Conformational analysis of the sugar ring in nucleosides and nucleotides. A new description using the concept of pseudorotation. *J. Am. Chem. Soc.*, **94**, 8205–8212.
51. Egli,M., Portmann,S. and Usman,N. (1996) RNA hydration: a detailed look. *Biochemistry*, **35**, 8489–8494.
52. Soler-Lopez,M., Malinina,L. and Subirana,J.A. (2000) Solvent organization in an oligonucleotide crystal. The structure of d(GCGAATTCG)$_2$ at atomic resolution. *J. Biol. Chem.*, **275**, 23034–23044.
53. Wang,P., Brank,A.S., Banavali,N.K., Nicklaus,M.C., Marquez,V.E., Christman,J.K. and MacKerell,J.A.D. (2000) Use of oligodeoxyribonucleotides with conformationally constrained abasic sugar targets to probe the mechanism of base flipping by *Hha* I DNA (cytosine C5)-methyltransferase. *J. Am. Chem. Soc.*, **122**, 12422–12434.